



**Michigan
Technological
University**

Michigan Technological University
Digital Commons @ Michigan Tech

Department of Physics Publications

Department of Physics

2-17-2012

Observational bounds on atmospheric heating by aerosol absorption: Radiative signature of transatlantic dust

Amit Davidi
Weizmann Institute of Science

Alexander Kostinski
Michigan Technological University

Ilan Koren
The Weizmann Institute of Science

Yoav Lehahn
Weizmann Institute of Science

Follow this and additional works at: <https://digitalcommons.mtu.edu/physics-fp>



Part of the [Physics Commons](#)

Recommended Citation

Davidi, A., Kostinski, A., Koren, I., & Lehahn, Y. (2012). Observational bounds on atmospheric heating by aerosol absorption: Radiative signature of transatlantic dust. *Geophysical Research Letters*, 39(4), 1-5.

<http://dx.doi.org/10.1029/2011GL050358>

Retrieved from: <https://digitalcommons.mtu.edu/physics-fp/195>

Follow this and additional works at: <https://digitalcommons.mtu.edu/physics-fp>



Part of the [Physics Commons](#)

Observational bounds on atmospheric heating by aerosol absorption: Radiative signature of transatlantic dust

Amit Davidi,¹ Alex B. Kostinski,² Ilan Koren,¹ and Yoav Lehahn^{1,3}

Received 14 November 2011; revised 11 January 2012; accepted 16 January 2012; published 17 February 2012.

[1] Aerosols absorb solar radiation thus changing the atmospheric temperature profile but the overall magnitude of this effect is not known. To that end, Saharan dust emissions over the Atlantic Ocean provide an opportunity to examine aerosol-related heating via satellite imaging. A major difficulty, however, is disentangling a straightforward heating signal caused by the absorbing dust from a meteorological signal, which originates from correlation between dust concentration and air temperature. To tackle the problem, we combine temperature (T) soundings, from the atmospheric infrared sounder (AIRS), with aerosol optical depth (τ) measurements, from the moderate resolution imaging spectroradiometer (MODIS), and data assimilation results from the global data assimilation system (GDAS). We introduce the quantity $\beta(P) \equiv \partial T_p / \partial \tau$, the subscript indicating temperature at a given pressure, and study the observed (AIRS) vs. modeled (GDAS) vertical profiles of $\beta(P)$. Using the vertical as well as horizontal patterns of $\beta(P)$ and $\Delta\beta(P) \equiv \beta_{obs.} - \beta_{mod.}$, we avoid instrumental and geographic artifacts and extract a remarkably robust radiative heating signal of about 2–4 K within the dust layer. The extracted signal peaks over the mid-Atlantic Ocean, as a result of competing trends: “memory” of the dust source in the east, and mixing with transparent aerosol in the west. **Citation:** Davidi, A., A. B. Kostinski, I. Koren, and Y. Lehahn (2012), Observational bounds on atmospheric heating by aerosol absorption: Radiative signature of transatlantic dust, *Geophys. Res. Lett.*, 39, L04803, doi:10.1029/2011GL050358.

1. Introduction

[2] Saharan dust, as any aerosol, interacts with solar radiation through scattering and absorption. While both processes are expected to cool the air below the aerosol layer, absorption is expected to cause heating within the layer (“radiative heating”). The magnitudes of the heating and cooling depend on the aerosol’s optical properties [Moosmüller *et al.*, 2009]. During the northern hemisphere summer (June–August) Saharan dust is being transported over the Atlantic Ocean [Prospero *et al.*, 2002]. The dust is lifted to an altitude of 3–5 km, and reaches the Americas in about a week [Ginoux *et al.*, 2004; Kaufman *et al.*, 2005; Schepanski *et al.*, 2009]. During this time of year the dust is relatively “pure”, i.e., not mixed with biomass-burning smoke [Ben-Ami *et al.*, 2009; Haywood *et al.*, 2008]. Saharan dust has single scattering albedo of

0.8–0.95, in the visible wavelengths [Dubovik *et al.*, 2002; Otto *et al.*, 2007], rendering it an absorbing aerosol.

[3] Recent studies [Davidi *et al.*, 2009; Wang, 2010] suggested that absorption might warm the aerosol layer by up to 2 K but did not address meteorological correlations. Indeed, if “dusty” air is warmer simply because it originated in the Saharan hot spots; the observed warming is not due to radiative heating. How does one separate the two effects?

2. Methods

[4] To that end, we examined the vertical profiles of temperature (T) and the aerosol optical depth (τ) over the mid Atlantic Ocean (Figure 1a) for the period June–August, 2003–2010 (only 2009 are presented in the main text; see remaining results in the auxiliary material).¹ The aerosol optical depth (τ) and cloud fraction data are taken from the moderate resolution imaging spectroradiometer (MODIS) instrument [Levy *et al.*, 2007; Remer *et al.*, 2008]. We use level 3, 1° by 1°, daily data; all AOD data is at 550 nm. Due to cloud contamination, we restricted the value of τ to below 0.6 [Brennan *et al.*, 2005]. Temperature profiles data are taken from 2 sources: the atmospheric infrared sounder (AIRS) [Aumann *et al.*, 2003] and the global data assimilation system (GDAS) [Kanamitsu, 1989]. From AIRS, we use global, level 3, 1° by 1°, daily data. Daily 0.25° wind speed data are derived from the advanced microwave scanning radiometer NASA’s - Earth Observing System (AMSRE). MODIS, AMSR-E and AIRS fly on the Aqua platform (overpasses at ~1:30 local time). The GDAS scheme produces global temperature maps at standard pressure levels (1000, 925, 850, 700 hPa, etc.) 4 times a day (0, 6, 12, and 18 UTC), 1° by 1° resolution. In order to be able to compare the 2 temperature datasets (GDAS and AIRS), we linearly interpolated to 13:30 local time, using the values at 2 nearest times.

[5] The remotely sensed temperature (using AIRS instrument, hereafter referred to as “observed”) vs. τ (taken from MODIS), at 4 pressure levels, is shown in Figure 1b. Using the linear fits in Figure 1b, we introduce and plot vertical profiles of the quantity $\beta_{obs.}(P) \equiv \partial T_{P,obs.} / \partial \tau$ (Figure 1c, blue curve), interpreted as a measure of radiative heating (negative values indicate cooling).

[6] Figure 1b is plotted by binning the dataset (~280 points per bin), and plotting the mean temperature versus the mean τ at each bin. The error bars are the 99% confidence interval of the mean. We note that hereafter all temperature changes are per unit τ (not absolute temperature).

3. Results

[7] In Figure 1, we see a cooling of ~1 K per unit τ at a pressure level of 1000 hPa (below the dust layer), heating of

¹Department of Environmental Science and Energy Research, Weizmann Institute of Science, Rehovot, Israel.

²Department of Physics, Michigan Technological University, Houghton, Michigan, USA.

³Department of Geophysics and Planetary Sciences, Tel Aviv University, Tel Aviv, Israel.

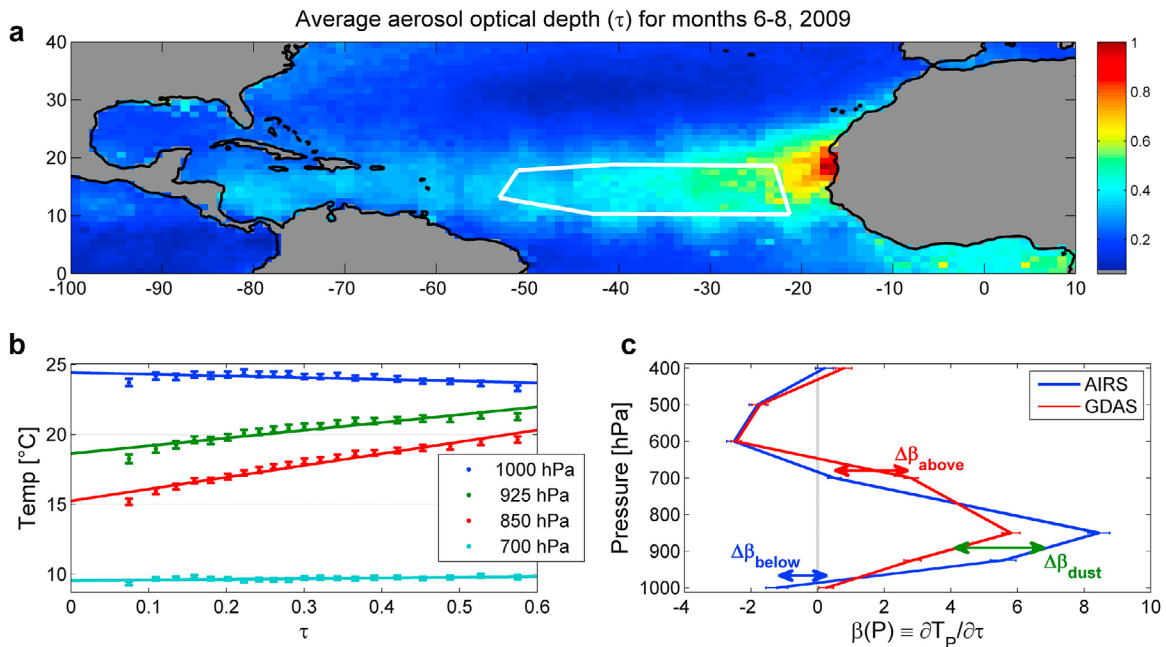


Figure 1. Detecting the radiative signal of transatlantic dust. (a) Mean aerosol optical depth (τ) for the summer months (June–August), 2009. The dust plume region is clearly visible. The white line delimits the study region. (b) Observed (binned) temperature at four pressure levels versus τ , for the region shown in Figure 1a. Each point is an average of ~ 280 pixels, and the average is within the error-bars at 99% confidence level. The straight lines are linear fits. (c) Vertical profiles of $\beta(P) \equiv \partial T_p / \partial \tau$; positive values of β indicate heating. Observe a cooling of ~ 1 K per unit τ at a pressure level of 1000 hPa (below the dust layer), heating of ~ 6 –8 K per unit τ at 925–850 hPa (within the dust layer), and cooling of ~ 2 K per unit τ at 600–500 hPa (above the dust layer). The blue curve was calculated using observed temperature profiles (from AIRS), while the red curve uses modeled data (from GDAS). The error bars indicate the 99% confidence region. The differences between the two curves serve as lower bound for the dust radiative signature: cooling below the dust layer, heating within it, and cooling above it ($\Delta\beta \equiv \beta_{\text{obs.}} - \beta_{\text{modl.}} < \beta_{\text{total}} - \beta_{\text{meteorology}} < \beta_{\text{dust}}$).

~ 6 –8 K per unit τ at 925–850 hPa (within the dust layer), and cooling of ~ 2 K per unit τ at 600–500 hPa (above the dust layer). While this is a physically appealing pattern, readily amenable to physical interpretation in terms of dust layer heating, a skeptical reader might argue that Figure 1 merely presents a correlation and need not imply causality. Indeed, one could propose four possible reasons for such correlations:

1. AIRS retrieval artifacts: dust particles are large enough (up to several microns in diameter) to be comparable to the IR wavelengths.

2. Geography: westward regions are colder (further from the warm Saharan Desert source) and have lighter dust loadings, due to progressive westward dilution of dust plumes by ambient air, thereby yielding temperature–dust correlations.

3. Meteorology: dust outbursts are associated with warm and dry air layer (known as Saharan air layer, SAL), thus the dust functions as a tracer of the warm air.

4. Aerosol radiative effect: dust absorbs and scatters solar radiation, thus heats the dust layer while cooling the layers below.

[8] We tackle option 1 first. While AIRS has been validated in numerous experiments [Gao *et al.*, 2008; Olsen *et al.*, 2007; Susskind *et al.*, 2006; Tobin *et al.*, 2006], no validation has been done specifically to examine the possible effects of dust aerosols [Nalli and Stowe, 2002]. However, one could not a-priori claim that dust aerosol will cause

biases, rather than only increasing retrieval noise (i.e., its root mean square, relative to a reference). Furthermore, even if dust is associated with inversion bias, sign-alternating biases at consecutive pressure levels appear rather unlikely. In other words, to yield the profile in Figure 1c, the artifacts must “conspire” for a net bias of alternating heating and cooling. Wang [2010] showed very similar heating patterns using completely different instruments (OMI and FORMOSAT-3/COSMIC), rendering this scenario even less plausible.

[9] In order to examine the geography-driven argument, we divided the Atlantic Ocean region to smaller boxes, going east to west (Figure 2a), and plotted the heating profiles, $\beta_{\text{obs.}}(P)$, for each box (Figure 2b). By dividing to smaller boxes, and remembering that $\beta(P)$ is the temperature change per unit τ , we are allowed to neglect, at least to first order, this mixing effect (which is the underlying essence of the geography argument). Thus, since the profiles seen in Figure 2b are different for each sub-region, with a clear trend – eastern boxes have significantly more positive heating profiles than western boxes – we claim that this “geography effect” is not the dominant factor in the correlation.

[10] The remaining meteorological and the aerosol radiative signals are closely coupled, making their disentanglement difficult. Ideally, one might try to tackle this problem by using a “perfect” model which “knows” about every atmospheric physical law, excluding the aerosol radiative effect. Then, by subtracting the observed heating profiles from the modeled ones, one could extract the pure dust

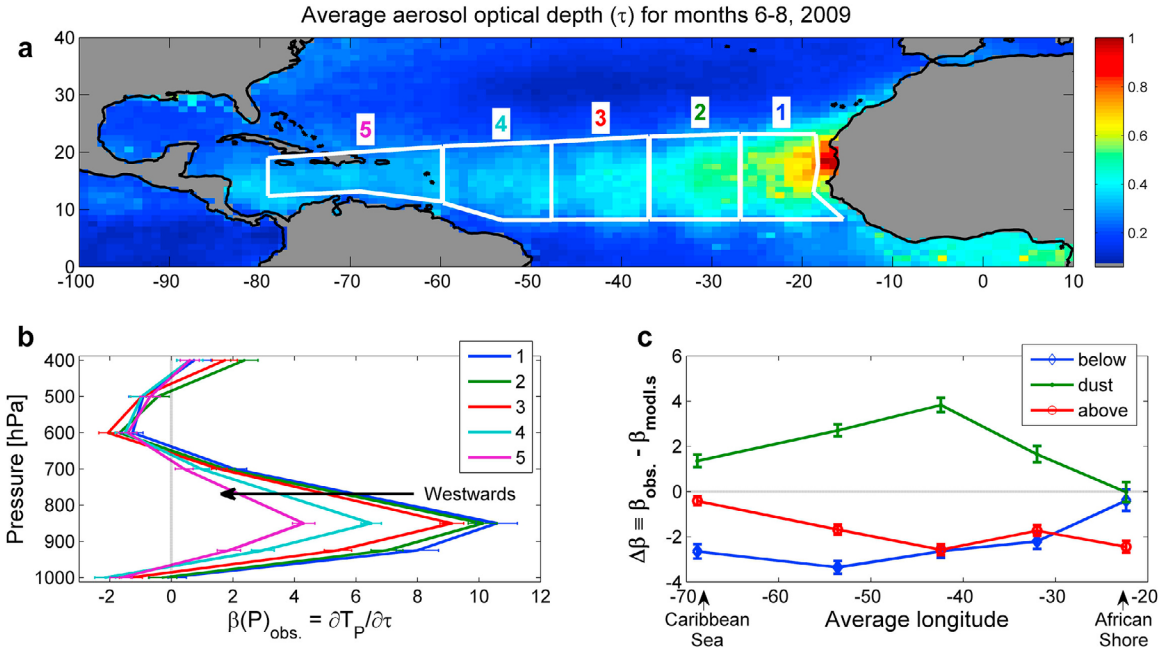


Figure 2. Vertical and horizontal patterns of the radiative signature. (a) Similar to Figure 1a, but dividing the Atlantic Ocean to 5 boxes, numbered 1 through 5, east to west. (b) $\beta_{obs.}(P)$ profiles for boxes 1 to 5, using AIRS temperature data. Eastern profiles are more pronounced, ruling out geographically induced correlation (see text). (c) $\Delta\beta$ ($\equiv \beta_{obs.} - \beta_{modl.}$) versus mean box longitude at three levels: below the dust layer (1000 hPa, blue curve), within the dust layer (925–850 hPa, green), and above the dust (700 hPa, red). As GDAS data may implicitly account for some of the dust absorption, the quantity $\Delta\beta$ furnishes a conservative (lower) bound for the magnitude of the dust radiative effects (heating or cooling). The presence of the peak heating at the dust layer (green curve) is, likely, an indication for two opposing trends: “memory” of the Saharan Desert source versus the mixing with the transparent (non-absorbing) aerosol of marine origin.

radiative signal. We used the global data assimilation system [Kanamitsu, 1989] (GDAS) as an approximation for that ideal model. GDAS is imperfect: it does not include all relevant atmospheric science (due to lack of knowledge and insufficient computational power). More importantly, dust radiative effect is indirectly incorporated into the GDAS data set, through the dust effect on the radiances and temperatures measured by remote sensing instruments and radiosondes. Figure 1c shows the heating profile derived from the GDAS data set (hereafter referred to as “modeled”), $\beta_{modl.}(P)$ (red curve). The profile roughly follows the observed heating profile (blue curve). As discussed above, the difference between the two curves can serve as a lower bound for the dust radiative signature (lower because dust radiative effects are indirectly incorporated into GDAS):

$$\begin{aligned} \Delta\beta &\equiv \beta_{obs.} - \beta_{modl.} \\ \Delta\beta &< \beta_{total} - \beta_{meteorology} \\ \Delta\beta &< \beta_{dust} \end{aligned}$$

To facilitate the interpretation of this new methodology, we ask: what is expected if meteorology is the only driving factor, i.e., dust serves as an air tracer of the hot Saharan air layer (SAL)? Then, the dust layer should show positive values of β , the layer above is expected to show negative values because of the enhanced (by drying) radiational cooling, etc. [see, e.g., Dunion and Marron, 2008, pp. 5248–5249], but the layers below the dust should show β values close to zero. These features are indeed seen in the model profile of Figure 1c (red curve). The negative $\beta_{obs.}$ value

below the dust layer, however, is an indication of a dust radiative signature.

[11] To zoom in on the essential physics we, therefore, examine the value of $\Delta\beta$ at 3 layers: below the dust (1000 hPa), within the dust layer (925–850 hPa), and right above the dust (700 hPa) [Ben-Ami et al., 2009]. Figure 1c illustrates the calculation of these 3 values and the spatial pattern of $\Delta\beta$ for these 3 layers is presented in Figure 2c. Note that since β , and therefore $\Delta\beta$, are normalized (units of temperature change per unit τ), dilution with the ambient air cannot be considered as an explanation for any trend observed, as explained above. The layer below the dust ($\Delta\beta_{below}$, blue curve) shows restricted cooling values, except for the eastern-most box (closest to the African shore), of about 2–4 K per unit τ . The dust layer ($\Delta\beta_{dust}$, green) displays a remarkably robust maximum: from no significant heating in box 1 (closest to the Africa shore), to a maximum value of ~ 4 K per unit τ at box 3 (middle of the Atlantic Ocean), and then a decrease to a value of ~ 1.5 K per unit τ at box 5 (the Caribbean Sea). The layer above the dust ($\Delta\beta_{above}$, red) shows cooling of ~ 2 K per unit τ , except for the western-most box. Note that previous studies showed heating of ~ 2 K [Davidi et al., 2009; Wang, 2010].

[12] The presence of the maximum suggests competing effects: the eastern-most region is the closest to the Sahara Desert, therefore the layer has the strongest “memory” of the SAL environment, so differentiating between meteorological and aerosol radiative effects is practically impossible. Thus getting further westwards enables better separation of the two signals. However, we argue that the western-most box

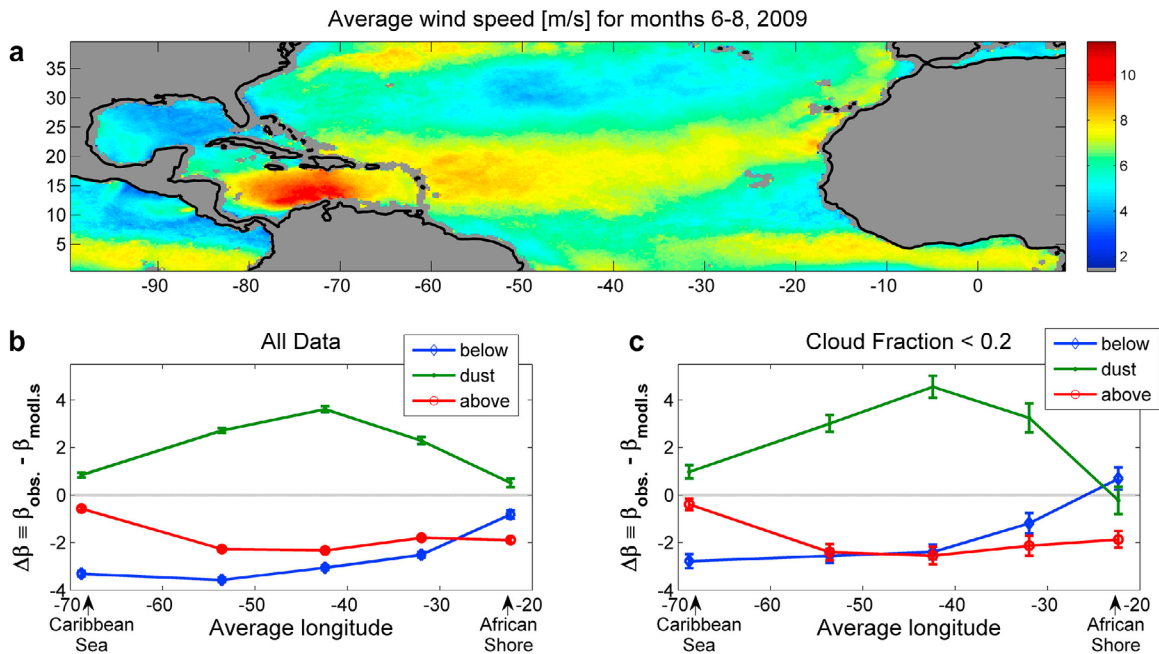


Figure 3. (a) Horizontal pattern of surface wind: Surface winds display longitudinal west to east gradient, with strongest winds over the Caribbean Sea. As the surface winds are tightly correlated with the marine aerosol, we argue that the weaker heating seen in the 2 western boxes (see Figure 2) is due to mixing with the marine non-absorbing aerosol. Robustness of the radiative signature. (b) Similar to Figure 2c, but combining data from June–August of years 2003–2010. (c) Restricting the data to pixels with cloud fraction below 0.2. Deviations between Figures 3b and 3c are within the error bars, indicating the robustness of the dust radiative signature with respect to the year or cloud fraction.

shows smaller heating (compared with the middle box) due to the presence of non-absorbing aerosol types, specifically marine aerosol. These transparent aerosols are located near the surface and do not absorb solar radiation, but they are included in the MODIS aerosol optical depth retrieval (τ). Since these aerosols are generated by the wind, stronger surface winds indicate higher concentrations of marine aerosol [Lehahn *et al.*, 2010]. Figure 3a shows the mean surface wind strength for the months June–August, 2009. It shows a clear gradient of the surface winds which results in higher non-absorbing aerosol concentrations in the western boxes. This supports our hypothesis that the decrease heating in the Caribbean Sea is due to the presence of marine non-absorbing aerosol.

[13] We note that one could hypothesize that since GDAS has radiosondes measurements at both eastern and western ends of the Atlantic Ocean (serving as “anchors”); the highest deviation is expected in the middle. Although this is possible, and might contribute somewhat to our analysis, it could not account for the entire maximum seen in Figure 2c. We also note that similar results were obtained for all years 2003–2010 (see Figures S1–S14), which points to the robustness of our methodology.

[14] So far we have ignored clouds altogether. Clouds might obscure the dust radiative effect by blocking the dust (depending, of-course, on their height), thereby diminishing the apparent dust heating. On the other hand, clouds could increase dust absorption through “photon bouncing” effects, i.e., reflecting solar radiation, thus increasing the optical path the light travels through the dust layer. This question remains open as our methodology cannot discern the effects.

[15] Ideally, one should scrutinize the data to a narrow cloud fraction values (e.g., only no-clouds pixels), but this approach causes a statistical problem since not enough data would remain. Therefore, we combined data from several years (Figure 3b). Note the similarity between Figures 3b and 2c, an indication for the robustness mentioned above, and a justification for merging all available summer data. Figure 3c is based on the same analysis, but restricting the data only to pixels with cloud fraction below 0.2 (for convenience, this data set will be termed “cloud-free”). As expected, the “cloud-free” data set is noisier (as indicated by the larger error bars), but the differences are within the error bars. The similarities between the “all-data” and the “cloud-free” data sets indicate that the dust radiative effect is quite robust.

4. Summary

[16] By combining data from two instruments and examining the proposed beta-signature, we found evidence for the radiative heating of the dust layer over the Atlantic Ocean of at least 2–4 K. Exploiting spatial patterns of AIRS and GDAS temperature profiles ruled out other causes. Dust absorption has a maximum along the east-west summer transport route, suggesting interplay of geographic memory and aerosol optical properties. Such significant absorption is expected to affect the stability of the atmospheric profile, suppressing cloud formation below the heated layer. Due to the sheer vastness and abundance of transatlantic dust, such effects are likely to be important and to affect the atmosphere on a synoptic and possibly global scale. Therefore,

desertification and changes in patterns of dust emissions are expected to change patterns of such effects.

[17] **Acknowledgments.** AMSR-E data are produced by Remote Sensing Systems and sponsored by the NASA Earth Science Measures Discover Project and the AMSR-E Science Team. Data are available at www.remss.com. This research was supported in part by the Israel Science Foundation (grant 1172\10). A. B. Kostinski was supported, in part, by NSF AGS-1119164.

[18] The Editor thanks an anonymous reviewer for his/her assistance in evaluating this paper.

References

- Aumann, H. H., et al. (2003), AIRS/AMSU/HSB on the aqua mission: Design, science objectives, data products, and processing systems, *IEEE Trans. Geosci. Remote Sens.*, *41*(2), 253–264, doi:10.1109/TGRS.2002.808356.
- Ben-Ami, Y., I. Koren, and O. Altaratz (2009), Patterns of North African dust transport over the Atlantic: Winter vs. summer, based on CALIPSO first year data, *Atmos. Chem. Phys.*, *9*(20), 7867–7875, doi:10.5194/acp-9-7867-2009.
- Brennan, J. I., Y. J. Kaufman, I. Koren, and R. R. Li (2005), Aerosol-cloud interaction-misclassification of MODIS clouds in heavy aerosol, *IEEE Trans. Geosci. Remote Sens.*, *43*(4), 911–915, doi:10.1109/TGRS.2005.844662.
- Davidi, A., I. Koren, and L. Remer (2009), Direct measurements of the effect of biomass burning over the Amazon on the atmospheric temperature profile, *Atmos. Chem. Phys.*, *9*(21), 8211–8221, doi:10.5194/acp-9-8211-2009.
- Dubovik, O., B. Holben, T. F. Eck, A. Smirnov, Y. J. Kaufman, M. D. King, D. Tanre, and I. Slutsker (2002), Variability of absorption and optical properties of key aerosol types observed in worldwide locations, *J. Atmos. Sci.*, *59*(3), 590–608, doi:10.1175/1520-0469(2002)059<0590:VOAAOP>2.0.CO;2.
- Dunion, J. P., and C. S. Marron (2008), A reexamination of the Jordan mean tropical sounding based on awareness of the Saharan air layer: Results from 2002, *J. Clim.*, *21*(20), 5242–5253, doi:10.1175/2008JCLI1868.1.
- Gao, W. H., F. S. Zhao, Y. F. Xu, and X. Feng (2008), Validation of the surface air temperature products retrieved from the atmospheric infrared sounder over China, *IEEE Trans. Geosci. Remote Sens.*, *46*(6), 1783–1789, doi:10.1109/TGRS.2008.916640.
- Ginoux, P., J. M. Prospero, O. Torres, and M. Chin (2004), Long-term simulation of global dust distribution with the GOCART model: Correlation with North Atlantic Oscillation, *Environ. Modell. Software*, *19*(2), 113–128.
- Haywood, J. M., et al. (2008), Overview of the Dust and Biomass-burning Experiment and African Monsoon Multidisciplinary Analysis Special Observing Period-0, *J. Geophys. Res.*, *113*, D00C17, doi:10.1029/2008JD010077.
- Kanamitsu, M. (1989), Description of the NMC Global Data Assimilation and Forecast System, *Weather Forecast.*, *4*(3), 335–342, doi:10.1175/1520-0434(1989)004<0335:DOTNGD>2.0.CO;2.
- Kaufman, Y. J., I. Koren, L. A. Remer, D. Tanre, P. Ginoux, and S. Fan (2005), Dust transport and deposition observed from the Terra-Moderate Resolution Imaging Spectroradiometer (MODIS) spacecraft over the Atlantic Ocean, *J. Geophys. Res.*, *110*, D10S12, doi:10.1029/2003JD004436.
- Lehahn, Y., I. Koren, E. Boss, Y. Ben-Ami, and O. Altaratz (2010), Estimating the maritime component of aerosol optical depth and its dependency on surface wind speed using satellite data, *Atmos. Chem. Phys.*, *10*, 6711–6720, doi:10.5194/acp-10-6711-2010.
- Levy, R. C., L. A. Remer, S. Mattoo, E. F. Vermote, and Y. J. Kaufman (2007), Second-generation operational algorithm: Retrieval of aerosol properties over land from inversion of Moderate Resolution Imaging Spectroradiometer spectral reflectance, *J. Geophys. Res.*, *112*, D13211, doi:10.1029/2006JD007811.
- Moosmüller, H., R. K. Chakrabarty, and W. P. Arnott (2009), Aerosol light absorption and its measurement: A review, *J. Quant. Spectrosc. Radiat. Transfer*, *110*(11), 844–878, doi:10.1016/j.jqsrt.2009.02.035.
- Nalli, N. R., and L. L. Stowe (2002), Aerosol correction for remotely sensed sea surface temperatures from the National Oceanic and Atmospheric Administration advanced very high resolution radiometer, *J. Geophys. Res.*, *107*(C10), 3172, doi:10.1029/2001JC001162.
- Olsen, E. T., E. Fetzer, S. Y. Lee, E. Manning, J. Blaisdell, and J. Susskind (2007), *AIRS/AMSU/HSB Version 5 CalVal Status Summary*, Jet Propul. Lab., Calif. Inst. of Technol., Pasadena.
- Otto, S., M. de Reus, T. Trautmann, A. Thomas, M. Wendisch, and S. Borrmann (2007), Atmospheric radiative effects of an in situ measured Saharan dust plume and the role of large particles, *Atmos. Chem. Phys.*, *7*(18), 4887–4903, doi:10.5194/acp-7-4887-2007.
- Prospero, J. M., P. Ginoux, O. Torres, S. E. Nicholson, and T. E. Gill (2002), Environmental characterization of global sources of atmospheric soil dust identified with the NIMBUS 7 Total Ozone Mapping Spectrometer (TOMS) absorbing aerosol product, *Rev. Geophys.*, *40*(1), 1002, doi:10.1029/2000RG000095.
- Remer, L. A., et al. (2008), Global aerosol climatology from the MODIS satellite sensors, *J. Geophys. Res.*, *113*, D14S07, doi:10.1029/2007JD009661.
- Schepanski, K., I. Tegen, and A. Macke (2009), Saharan dust transport and deposition towards the tropical northern Atlantic, *Atmos. Chem. Phys.*, *9*(4), 1173–1189, doi:10.5194/acp-9-1173-2009.
- Susskind, J., C. Barnet, J. Blaisdell, L. Iredell, F. Keita, L. Kouvaris, G. Molnar, and M. Chahine (2006), Accuracy of geophysical parameters derived from Atmospheric Infrared Sounder/Advanced Microwave Sounding Unit as a function of fractional cloud cover, *J. Geophys. Res.*, *111*, D09S17, doi:10.1029/2005JD006272.
- Tobin, D. C., H. E. Revercomb, R. O. Knuteson, B. M. Lesht, L. L. Strow, S. E. Hannon, W. F. Feltz, L. A. Moy, E. J. Fetzer, and T. S. Cress (2006), Atmospheric Radiation Measurement site atmospheric state best estimates for Atmospheric Infrared Sounder temperature and water vapor retrieval validation, *J. Geophys. Res.*, *111*, D09S14, doi:10.1029/2005JD006103.
- Wang, K.-Y. (2010), Profiles of the atmospheric temperature response to the Saharan dust outbreaks derived from FORMOSAT-3/COSMIC and OMI AI, *Atmos. Res.*, *96*(1), 110–121, doi:10.1016/j.atmosres.2009.11.017.

A. Davidi and I. Koren, Department of Environmental Science and Energy Research, Weizmann Institute of Science, PO Box 26, Rehovot 76100, Israel. (ilan.koren@weizmann.ac.il)

A. B. Kostinski, Department of Physics, Michigan Technological University, 1400 Townsend Dr., Houghton, MI 49931-1295, USA.

Y. Lehahn, Department of Geophysics and Planetary Sciences, Tel Aviv University, PO Box 39040, Tel Aviv 69978, Israel.